catalysts

MDPI

Communication

Enhanced Selective Production of Carbonyl Products for Aerobic Oxidation of Benzylic Alcohols over Mesoporous Fe_2O_3 Supported Gold Nanoparticles

Yanjun Jia [1,2,*] and Hanning Chen [1]

[1] School of Mechanical Engineering, Tianjin Polytechnic University, Tianjin 300387, China
[2] State Key Laboratory of Separation Membrane and Membrane Processes, Tianjin Polytechnic University, Tianjin 300387, China
* Correspondence: jiayanjun@tjpu.edu.cn; Tel.: +86-22-8395-5687

Received: 1 August 2019; Accepted: 1 September 2019; Published: 8 September 2019

Abstract: Ordered mesoporous Fe_2O_3 supported gold nanoparticles with a desired specific surface area and porous structure (Au/meso-Fe_2O_3) was successfully fabricated with a hard templating method by using KIT-6 as the template. The morphology and physico-chemical properties of Au/meso-Fe_2O_3 were characterized by X-ray diffraction (XRD), scanning electron microscope (SEM) and transmission electron microscope (TEM), etc. The gold nanoparticles are highly dispersed on the surface of the mesoporous Fe_2O_3. The catalytic performance of the synthesized catalyst was studied for the aerobic oxidation of benzylic alcohols in β–O–4 linked lignin model dimers to the corresponding carbonyl products under atmosphere pressure. Au/meso-Fe_2O_3 shows an enhanced activity for the aerobic oxidation of 1-phenylethanol in comparison with that of Au/bulk-Fe_2O_3. The promoted catalytic activity is related to the confined porous structure of mesoporous Fe_2O_3 and more boundaries contact between gold and meso-Fe_2O_3, which shows that the porous structure of the support has a significant influence on the activity of gold catalysts.

Keywords: mesoporous Fe_2O_3; gold nanoparticles; aerobic oxidation

1. Introduction

Lignin is a highly oxygenated and heterogeneous biopolymer, which comprises ~15–30 wt% of the biomass and ~40% of its total energy content [1,2]. As the largest renewable source of aromatics, lignin is the least utilized kind of lignocellulose due to its high strength and stability of aryl ether bonds and the rigid and compact structure thus formed, which results in recalcitrance to chemical processing [3]. It is highly challenging in terms of the selective depolymerization of lignin and is an active field of research [4,5]. At present, mild delignification methods, such as oxidative and hydrogenolytic procedures, have made encouraging progress, especially in terms of catalytic oxidative ways. Many recent studies focused on homogeneous methods, which show promising results. However, this is often more difficult for homogeneous catalysts used under a pilot-scale industrial application, due to the problems of poor selectivity and the difficulty in recovering the catalyst [6–8]. Heterogeneous oxidation systems, such as Cu, Pd, and Mo, have shown moderate to high yields for lignin model compounds and monoaromatic substrates [9–11]. However, the random distribution of active sites results in a wide distribution of products and decreases the stability of the catalysts [12–14]. In addition, the relatively poor mass transfer also decreased the oxidative activities of lignin-derived aromatic compounds, particularly for high biopolymer molecules, since in this case, quite a few aromatic compounds could adsorb to the surface of the metal active sites [15,16].

Herein, the aerobic oxidation of benzylic alcohols in β–O–4 linked lignin model dimers were catalyzed by ordered mesoporous Fe_2O_3 supported gold metal oxides (Au/meso-Fe_2O_3) with KIT-6

as a hard template under atmosphere pressure. As a highly ordered mesoporous silica, KIT-6 has two sets of enantiomeric interwoven mesopores with a 3-D cubic *Ia3d* arrangement of branched nanorods organized in KIT-6 mesoporous silica [17]. With the characterizations of X-ray diffraction (XRD), scanning electron microscope (SEM) and transmission electron microscope (TEM), etc., the gold nanoparticles are highly dispersed on the surface of the mesoporous Fe_2O_3. Additionally, the aerobic oxidation activities of Au/meso-Fe_2O_3 for benzylic alcohol are much higher than those of Au/bulk-Fe_2O_3 [18,19]. The mesostructures of the catalysts improved the oxidative performance by providing a high distribution of gold active sites [20], and the mesopores could enable the efficient transport of reactants and products to the catalytic sites [21,22].

2. Results and Discussion

2.1. Characterization of the Catalysts

To investigate and certify the mesoporous structure of Au/meso-Fe_2O_3 composite oxides (Au/meso-Fe_2O_3), the low-angle XRD patterns of pure-silicon KIT-6, as-made meso-Fe_2O_3, Au/meso-Fe_2O_3 and post-reaction Au/meso-Fe_2O_3 are shown in Figure 1A [23]. From Figure 1A, all samples exhibited a prominent peak at 1.1 degree and two weak peaks consistent with the diffraction pattern of KIT-6, corresponding to the (211) and (220) reflections, respectively [24]. These results indicated that the obtained Au/meso-Fe_2O_3 replicated the ordered mesoporous structure of KIT-6 templates excellently, even after the impregnation with the metallic species and the calcination processes [23,25]. Compared with the original KIT-6, the diffraction peak intensity of the catalysts after incorporation into the metal species was decreased, which was attributed to the decrease in the electron density during the reaction process when the metal species leaching entered the KIT-6 channels [26,27]. Figure 1B shows the high-angle XRD patterns of Au/bulk-Fe_2O_3, meso-Fe_2O_3, Au/meso-Fe_2O_3 and postreaction Au/meso-Fe_2O_3. From Figure 1B, the diffraction peak of Au/meso-Fe_2O_3 is relatively broader than that of Au/bulk-Fe_2O_3, which might be due to the reduced crystallinity of the Au/meso-Fe_2O_3 and the existence of small particles in the pore walls. There are no detectable characteristic peaks of Au in all the catalysts, which is mainly due to the low content and small size of Au (lower than 4 nm). The diffraction patterns of the spent Au/meso-Fe_2O_3 remain unchanged, indicating the rather good stability of Au/meso-Fe_2O_3. To conclude, the Au/meso-Fe_2O_3 material has a mesoporous morphology, and gold metal has a good dispersion on the surface of the mesoporous catalyst. The formation of a good mesoporous channel provides a way to react with the active sites for the large size of the lignin model molecules, which has laid a good foundation for the further degradation of lignin.

In order to further study the morphology and textural property of the catalyst, Au/meso-Fe_2O_3 and post-reaction Au/meso-Fe_2O_3 were characterized by SEM (Figure 1C). The porous structure of Au/meso-Fe_2O_3 could be observed, and the particle size of the catalyst was about 5–10 μm, which maintains the similar surface morphology of the KIT-6 templates. The morphology and structure of Au/meso-Fe_2O_3 were also characterized by TEM (Figure 1D). From Figure 1D, the well-ordered mesoporous structure of the KIT-6 silica template was successfully replicated on Au/meso-Fe_2O_3. Au/meso-Fe_2O_3 has a high crystallinity and uniform *Ia3d*-type cubic mesostructures replicated from the KIT-6 templates [23,28]. The TEM images of Figure 1D show the structure of the Au nanoparticles encapsulated by the mesoporous Fe_2O_3. The corresponding Au particle size distribution showed a median particle size of 2.7 nm. The obtained gold particle size is very similar to an average value. As a matter of fact, this preparation method results in a very small and homogeneous gold particle size distribution (~2.7 nm, lower than 4 nm), which indicates that the synthetic method is reliable for the preparation of small metal nanoparticles [29]. The successful synthesis of the catalyst Au/meso-Fe_2O_3 could be found with hard template methods, which is further confirmed by the XRD and following BET surface area results.

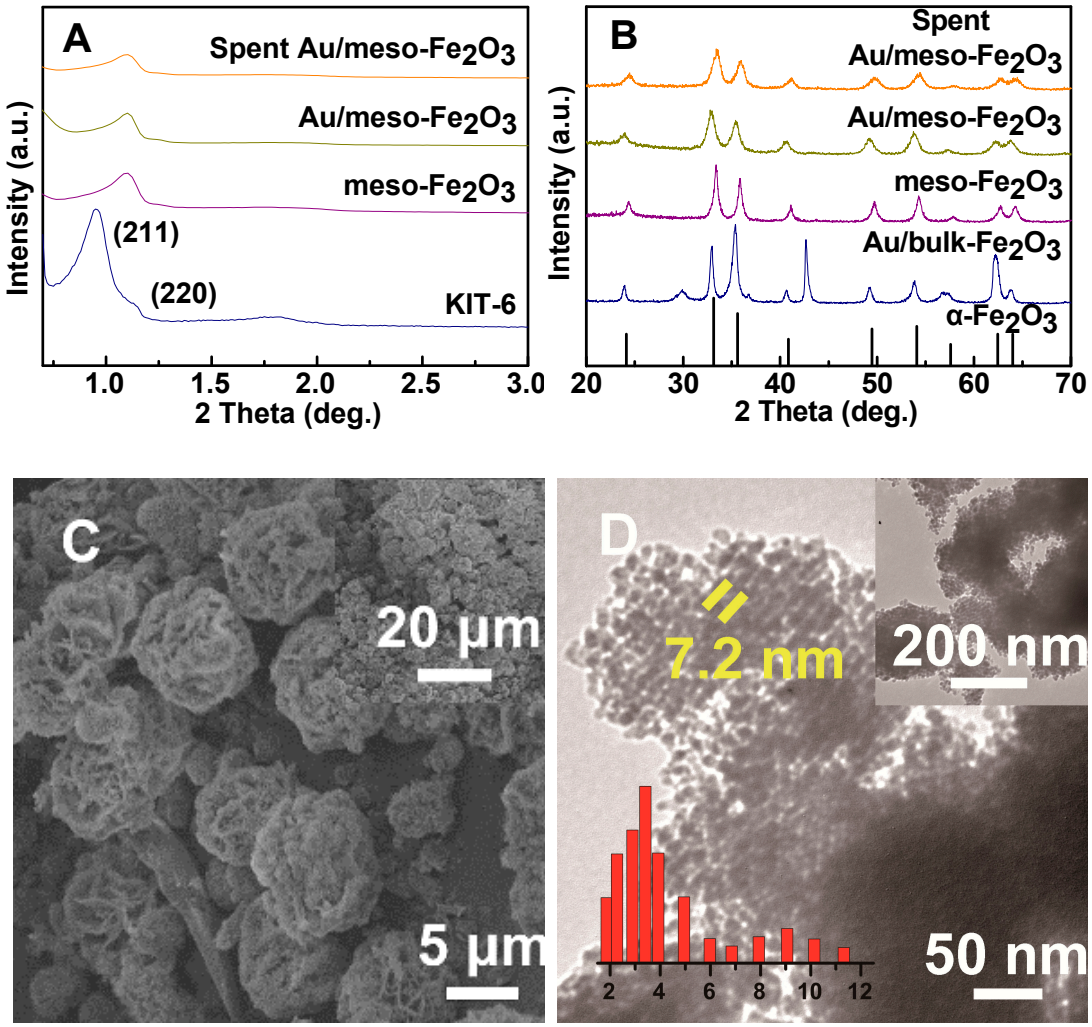

Figure 1. (**A**) Low-angle and (**B**) high-angle X-ray diffraction (XRD) patterns of different iron-based catalysts, (**C**) scanning electron microscope (SEM) images and (**D**) transmission electron microscope (TEM) images of mesoporous Fe_2O_3 supported gold nanoparticles (Au/meso-Fe_2O_3).

The textural properties of the Au/meso-Fe_2O_3 catalysts were studied by a nitrogen adsorption analysis, which is shown in Table 1. From Table 1, the Au/meso-Fe_2O_3 obtained by the incorporation of metal species into the pores of KIT-6 was 97.2 $m^2 \cdot g^{-1}$ and 9.1 nm in the specific surface area and average pore diameter. From the pore size distribution analysis of Au/meso-Fe_2O_3, the pore size distribution of the catalyst was still uniform, which is in agreement with the XRD results [20,27]. The Au/meso-Fe_2O_3 catalyst still exhibits typical type IV isotherms with a mesoporous structure [30,31]. The retention of this kind of pore is beneficial for the diffusion of lignin into the catalyst, which can enhance mass transport and react with the catalytic active sites [32].

Combined with the XRD characterization of Au/meso-Fe_2O_3, the Brunauer–Emmett–Teller (BET) surface area of spent Au/meso-Fe_2O_3 was similar to the fresh one, which indicates the robust mesoporous structure and high recycling ability of the catalyst. Other important element contents (especially the Na and Si) were also analyzed with the inductive coupled plasma emission spectrometer (ICP) method. From Table 1, the sodium contents of all the mesoporous catalysts were lower than 0.02 wt% of fresh Au/meso-Fe_2O_3. After recycling the catalyst, the Na content decreased to 0.009 and 0.005 for the first and second runs, respectively. The Si contents also show similar trends to Na, which might be in favor of the aerobic oxidation of benzylic alcohol.

Table 1. The structural and chemical properties of Au/meso-Fe_2O_3 and selected iron-based catalysts.

Catalysts	S_{BET} [a] ($m^2 \cdot g^{-1}$)	D_p [b] (nm)	d_{XRD} (nm) [c]	Au wt% [d]	Na wt%	Si wt%	Au Leaching [e] ($mg \cdot L^{-1}$)
Au/bulk-Fe_2O_3	0.57	-	36.3	0.23	N/D	N/D	<0.1
Au/meso-Fe_2O_3	97.2	9.1	9.7	0.26	0.02	0.13	<0.1
Recycled 2nd Au/meso-Fe_2O_3	93.1	9.0	10.1	0.24	0.009	0.11	<0.1
Recycled 3rd Au/meso-Fe_2O_3	91.4	8.7	10.3	0.24	0.005	0.09	<0.1

[a] S_{BET}: surface area calculated by the BET method. [b] D_p: Barrett–Joyner–Halanda (BJH) average pore size calculated on the adsorption branch. [c] X-ray diffraction patterns (XRD). [d] Actual gold, sodium and silicon content in catalysts (wt%) determined by an inductive coupled plasma emission spectrometer (ICP)analysis. N/D stands for not detected. [e] Dissolved gold content in the solution after the reaction determined by the ICP analysis.

2.2. Oxidation of Benzylic Alcohols

The initial studies focused on the oxidation of 1-phenylethanol to compare the potential abilities of selected iron-based catalysts (shown in Table 2). By employing Au/meso-Fe_2O_3 as a catalyst, the activity and selectivity for benzylic alcohol oxidation increased significantly compared to Au/bulk-Fe_2O_3. The high oxidation activity of Au/meso-Fe_2O_3 could be explained by the porous structure of the Fe_2O_3 support and highly active site distribution of gold nanoparticles, which enhanced the mass transfer of reactants and products. Besides the porous nature of the Fe_2O_3 support, the size of gold nanoparticle also plays an important role. It is well known that the oxidation performance of alcohol could decrease significantly when the size of the gold nanoparticle surpasses 5 nm [25,26]. From Figure 1, we observe that most gold nanoparticles in Au/meso-Fe_2O_3 are <5 nm, hardly to be detected through the XRD characterizations. Since the gold nanoparticles are highly distributed on the mesoporous Fe_2O_3 surface, Au/meso-Fe_2O_3 could show an enhanced alcohol oxidation performance. Meanwhile, the Au/meso-Fe_2O_3 used in this catalyst system possesses an abundant mesoporous morphology with a relatively high surface area, which favors the adsorption of the alcohol and formation of small gold nanoparticles on the surface of the mesoporous Fe_2O_3. To investigate the Na contamination effects on the activity/selectivity of the Au/meso-Fe_2O_3, we further investigated the catalytic performance of fresh and recycled catalysts. If the Na contamination could seriously affect the activity/selectivity of the Au/meso-Fe_2O_3, the catalyst performance would dramatically decrease. The Na contents decreased to 0.009 wt% and 0.005 wt% after recycling for the first and second runs, respectively. Meanwhile, the oxidation activities of these catalysts remained similar (>99%) after recycling for two runs, which shows a stable catalytic conversion and selectivity for the oxidation of benzylic alcohol. The above results indicated that the contamination effect was not obvious, and was even negligible, for the aerobic oxidation of benzylic alcohol with Au/meso-Fe_2O_3. The reason for this may be the low Na content with the hard template synthetic method. Jiao et al. also reported similar results, where, after thorough etching and washing processes, the residue Na and Si content after nanocasting processes could be quite low for iron oxides [16]. To further verify this problem, we also carried out the experiments to add 1 wt% of $NaNO_3$ into Au/meso-Fe_2O_3 to poison the surface. The activity was significantly reduced to 13% under the same reaction conditions. The activity of the recycling test for this catalyst was also lower than that of Au/meso-Fe_2O_3. From the above results, a low Na content (<0.009%) has a low poison effect for the aerobic oxidation of Au/meso-Fe_2O_3. A high Na content (>1%) could greatly decrease the catalytic performance of the aerobic oxidation of Au/meso-Fe_2O_3. Therefore, there should be no Na contamination issue for the aerobic oxidation of benzylic alcohol with the Au/meso-Fe_2O_3.

Table 2. Oxidation of 1-phenylethanol to acetophenone using mesoporous iron-based catalysts [a].

Catalyst	Catalyst Dosage (mol%)	Temp. [°C]	t [h]	Conv. [b] [%]	Sel. [b] [%]
Meso Fe_2O_3	0.5	80	4	7	73
Au/bulk- Fe_2O_3	0.5	80	4	39	96
Au/meso- Fe_2O_3	0.5	80	4	99	>99
Recycled 2nd Au/meso-Fe_2O_3	0.5	80	4	99	>99
Recycled 3rd Au/meso-Fe_2O_3	0.5	80	4	99	>99
Au/meso-Fe_2O_3 with 1 wt% Na	0.5	80	4	13	87

[a] 1-Phenylethanol (1 mmol), diphenyl ether (10 mL), catalyst (0.2 g), 80 °C, p = 1 atm. air (30 mL·min^{-1}). [b] The conversion and selectivity were determined by gas chromatography-mass spectrometer (GC-MS) using dodecane as the internal standard.

In addition, Au/meso-Fe_2O_3 can also oxidize a wide range of benzylic alcohol to their corresponding carbonyl compounds with a high activity and selectivity, implying a high versatility of the catalyst. The Au/meso-Fe_2O_3 presents comparable activities, not only for benzylic secondary alcohols containing 1-phenylethanol and benzhydrol (Table 3, entries 1 and 7), but also for aliphatic secondary alcohols (Table 3, entry 8), compared with previously reported catalysts (Table 3, entries 2–6) at a high conversion. The oxidation of the hydroxyl group could be carried out with no cleavage of the cyclopropyl ring (entry 6). Moreover, Au/meso-Fe_2O_3 displays a higher selective oxidation activity for benzylic primary alcohols (Table 3, entry 10). We also note that Au/meso-Fe_2O_3 shows a high oxidation activity for allylic alcohols; for example, cinnamyl alcohol can be selectively oxidized to cinnamyl aldehyde with >99% selectivity in 4 h (Table 3, entry 9). The reactivity for benzylic alcohols is higher than for allylic and aliphatic ones. All these results indicate that the present catalysts are highly effective for the aerobic oxidation of alcohols under ambient air conditions. The oxidation activity of 1-phenylethanol for Au/meso-Fe_2O_3 was independent of the O_2 pressure, since the oxidation activity and selectivity of 1-phenylethanol remains similar under 0.2 (air), 1, 2 and 3 atm of molecular oxygen pressure.

Table 3. Aerobic oxidation of benzylic alcohols over Au/meso-Fe_2O_3 with air.

Entry	Substrate [a]	Temp. [°C]	Time [h]	Conv. [%] [b]	Product	Sel. [%] [c]
1	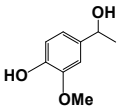	80	8	73	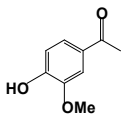	83
2	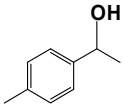	80	4	95	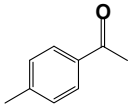	99
3	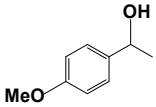	80	1	>99	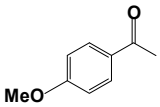	>99
4	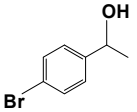	80	4	78	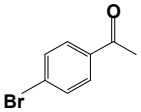	>99
5	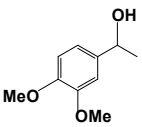	80	8	71	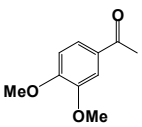	>99

Table 3. *Cont.*

Entry	Substrate [a]	Temp. [°C]	Time [h]	Conv. [%] [b]	Product	Sel. [%] [c]
6	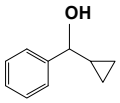	80	4	>99	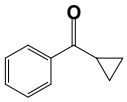	>99
7	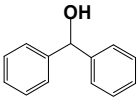	80	1	>99	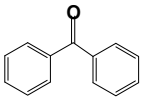	>99
8	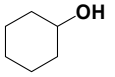	80	8	>99		>99
9	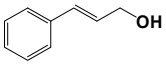	80	4	87	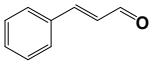	>99
10	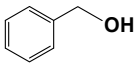	80	8	>99	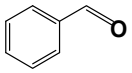	>99
11 [d]	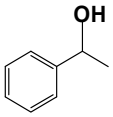	80	4	99	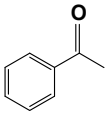	>99
		80		99		>99

[a] Substrate (1 mmol), catalyst (100 mg), diphenyl ether (10 mL), 80 °C, p = 1 atm. air (30 mL·min^{-1}). [b] The conversion were determined by GC-MS using dodecane as the internal standard. [c] The selectivity of products calculated by conversion and GC-MS analysis. [d] recycling reaction results of the 2nd and 3rd runs.

Upon consideration of the above results, the activation of O_2 represents one of the main difficulties for the rate limiting factors in alcohol oxidation [27]. Gold nanoparticles adsorbed on the surface of a porous support contain coordinatively unsaturated gold atoms, which are efficient for O_2 dissociation and activation. Electron-rich gold nanoparticles activate molecular oxygen via electron donation to the O_2. Meanwhile, a deprotonation of the benzylic hydroxyl group on the mesoporous Fe_2O_3 surface affords the adsorption of the Fe-alkoxide intermediate, following the Brønsted acid–base reaction patterns [33]. Through a series of deprotonation, elimination and catalyst regeneration steps, the presence of the mesoporousFe_2O_3 support provides a uniform distribution of Fe^{3+}, which is the key factor for the β–H elimination of metal alkoxide by the strong synergistic effect between the nearly atomically precise gold nanoparticles and the support. Meanwhile, the high activity and selectivity of the Au/meso-Fe_2O_3 can be related to the mesoporous morphology of the Fe_2O_3 support being favorable to the high dispersion of gold nanoparticles. Three batch reaction cycles have been tested for the gold nanoparticles after separation, and no activation loss of the catalyst has been found (Table 3, entry 11). Moreover, no Au and Fe leached into the supernatant, as confirmed by an ICP analysis, and almost the same particle size (10.1 and 10.3 nm for the 2nd and 3rd batches, respectively) and porous structure (9.0 and 8.7 nm, respectively) remained, as evidenced by XRD and the N_2-sorption of the reclaimed catalyst [30].

The reaction profiles for the oxidation of 1-phenylethanol was shown in Figure 2. Au/meso-Fe_2O_3 had an induction period of about 5 min. After this initial induction period, the molar ratio of the O_2 uptake to the acetophenone yield was ca. 1:2. The recyclability and stability of Au/meso-Fe_2O_3 are also important points to consider, especially when the industrial scale-up application of alcohol oxidations is used [31]. To test the lifetime profile of Au/meso-Fe_2O_3, another portion of the alcohol with the same amount was added to the reaction mixture after the first run. From Figure 2, the second and third cycles proceeded efficiently without any induction period, and acetophenone was obtained in a yield of over 99%. In addition, the catalyst was filtered off when the conversion was ca. 50% at the reaction temperature. After the catalyst was separated from the reaction system, the continued stirring of the filtrate under the same conditions did not give any products. The ICP analysis of

the filtrate confirmed that the contents of Au and Fe were below the detection limit. These results confirm that the oxidation occurred on the gold nanoparticles loaded on the surface of the mesoporous Fe_2O_3 [19,25]. After the first batch reaction, the catalyst was separated from the reaction mixture, thoroughly washed with toluene, and another portion of 1-phenylethanol were added under the same reaction conditions. The third batch reaction gave acetophenone in an over 99% conversion and 99% yield. These findings clearly suggest an excellent structural stability and recycling efficiency of the present ordered mesoporous Fe_2O_3 supported gold metal oxides catalyst.

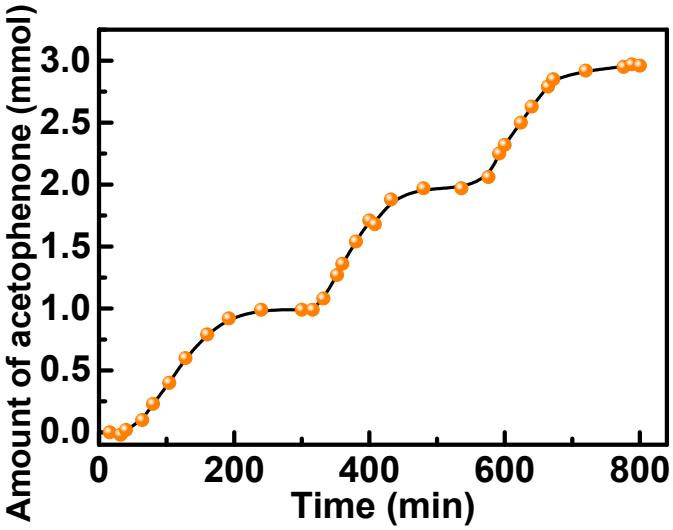

Figure 2. The time profile for the successive oxidation of 1-phenylethanol with Au/meso-Fe_2O_3. Reaction conditions: 1-phenylethanol (1 mmol), catalyst (100 mg), diphenyl ether (10 mL), 80 °C, p = 1 atm. air (30 mL·min^{-1}).

As mentioned with many reports, we compared the catalytic performance and reaction conditions with other results reported in the literature (Table 4). We note that Au/meso-Fe_2O_3 could oxidize 1-phenylethanol with a high conversion and relatively low catalyst dosage. In particular, compared to the gold nanoparticle supported on the Al_2O_3, TiO_2 and SiO_2, Au/meso-Fe_2O_3 showed enhanced catalyst activities (Entries 7, 9, and 11). After the addition of mesoporous Fe_2O_3, the gold nanoparticles on the surface of the mesoporous Fe_2O_3 could show a high aerobic oxidation of benzylic alcohol with a relatively low catalyst dosage.

Table 4. Aerobic oxidation of 1-phenylethanol over various Au catalysts.

Entry	Catalyst	Catalyst Dosage (mol%)	Time (h)	T (°C)	Conv. (%)	Sel. (%)	Ref.
1	Au/NiAl-LDH	0.01	1	160	19.5	>99	[31]
2	Au/ETS-10	0.03	6	160	42	>99	[34]
3	Au/$CuMgAl_4O_x$	0.09	1	90	85	>99	[35]
4	Au/NiAl-LDH	0.2	1	80	58.7	>99	[24]
5	Au/γ-Fe_2O_3/NiAl-LDH	0.2	1.5	80	95.8	>99	[24]
6	Au/LDH	0.5	12	20	96	>99	[36]
7	Au/Al_2O_3	0.9	4	100	5.5	>99	[37]
8	Au/FeO_x-Al_2O_3	0.9	4	100	52	>99	[37]
9	Au/TiO_2	0.9	4	100	9.4	>99	[37]
10	Au/FeO_x-Al_2O_3	0.9	4	80	25	>99	[37]
11	Au/SiO_2	1	4.5	90	74	>99	[38]
12	Au/sPSB	4	24	25	99	>99	[39]
13	Nanoporous Au	10	10	60	88	>99	[40]
14 [a]	Au/meso-Fe_2O_3	0.5	4	80	99 [b]	>99	This work

[a] Substrate (1 mmol), catalyst (100 mg), diphenyl ether (10 mL), 80 °C, p = 1 atm. air (30 mL·min^{-1}). [b] The conversion and selectivity were determined by GC-MS using dodecane as the internal standard.

For the catalytic oxidation process, many recent studies focused on the direct oxidation of lignin, where the wide product distribution increased the difficulties of following the separation processes [41]. The aerobic oxidation of Au/meso-Fe_2O_3 for benzylic alcohols in β–O–4 linked lignin model dimers was further investigated in Figure 3. Au/meso-Fe_2O_3 showed a high selectivity for the oxidation of the secondary benzylic alcohol with a nearly complete conversion of 96% in 12 h. Product **2** further reacted under the same conditions and give the dehydration product **3** and the retro-aldol product **4**. Product **4** reached a maximum yield of 25% and both guaiacol (product **5**) and p-anisic acid (product **6**) were produced, which was also confirmed by previous literature under aerobic conditions [42]. With Au/meso-Fe_2O_3 as a catalyst, the hydroxyl group of the Cα position was oxidized, which significantly lowered the C–O bond energy in the ketone form compared to the initial benzylic alcohol form [43]. Finally, products **5** and **6** reacted to form product **7** under esterification with a low yield. Since the esterification is undesirable and reversible, the product **7** could be cleaved by a simple hydrolysis method. As mentioned from the above results, Au/meso-Fe_2O_3 could effectively cleave the β–O–4 linked lignin model dimers with a high aromatic selectivity.

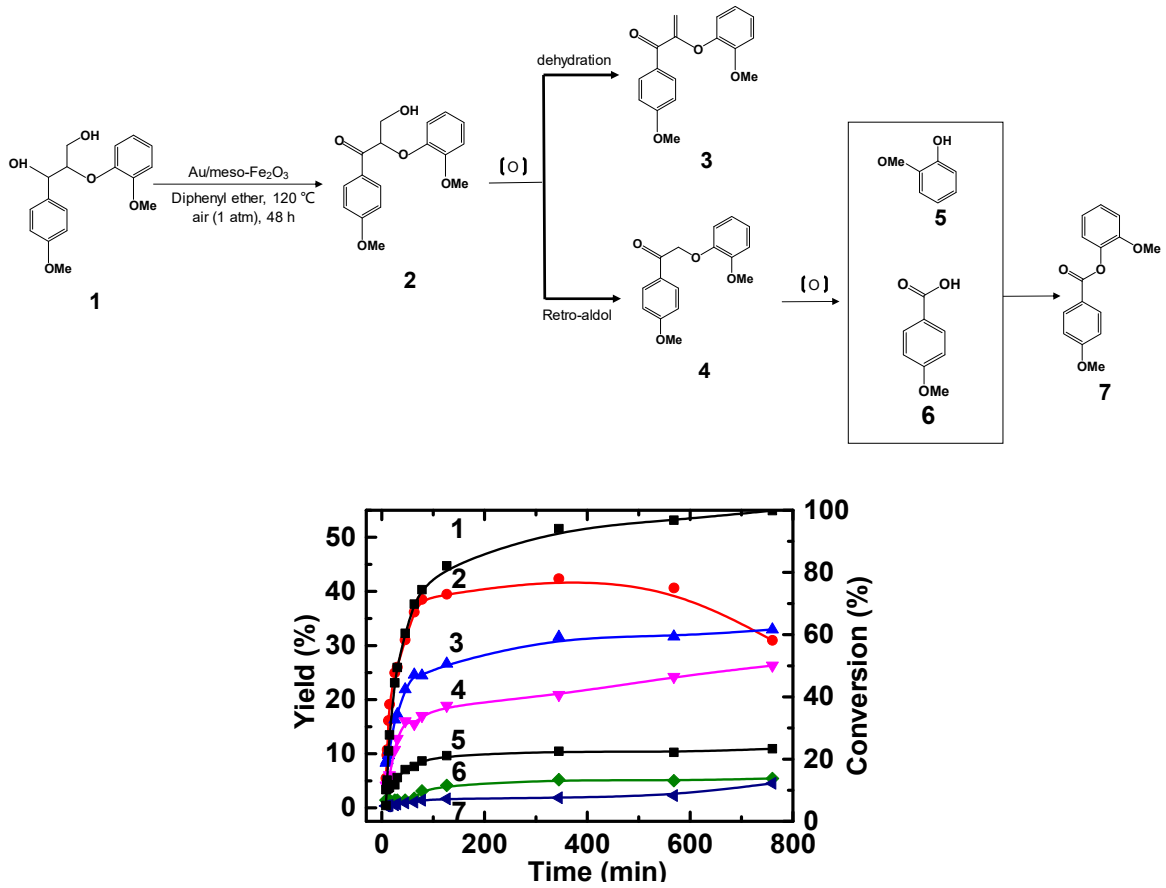

Figure 3. The aerobic oxidation of the lignin model dimer using Au/meso-Fe_2O_3. Conditions: substrate (1 mmol), catalyst (100 mg), diphenyl ether (10 mL), 120 °C, p = 1 atm. air (30 mL·min^{-1}). The conversion and yields were determined by GC-MS using dodecane as the internal standard.

3. Materials and Methods

3.1. Preparation of Catalysts

The mesoporous Fe_2O_3 supported gold nanoparticles (Au/meso-Fe_2O_3) were synthesized with a hard template method [24,44]. For the typical synthesis processes, 0.6 g KIT-6 was dispersed in 5 mL toluene by sufficient stirring and evenly dispersed, after which 1.1543 g $Fe(NO_3)_3{\cdot}9H_2O$ were added dropwise and refluxed for 6 h at 70 °C. Then, the solid mixture was filtrated, dried at 70 °C

and calcined at 600 °C with a heating rate of 1 °C·min^{-1} for 3 h. Finally, the resulting material was dissolved in 2 mol·L^{-1} NaOH and continuously stirred for 24 h at 40 °C. After washing and vacuum drying, the obtained mesoporous Fe_2O_3 was denoted as meso-Fe_2O_3 [23,28]. Then, 1 g of meso-Fe_2O_3 was added into 80 mL of water and stirred for 1 h. 10 mL of 0.0025 mol L^{-1} $HAuCl_4$ solution was added into the above solution and stirred for another 1 h. After adding $0.9 \times g$ of urea into the above mixture, the mixture was heated to 80 °C and continuously stirred for 8 h. After centrifuging and washing, the precipitate was vacuum dried at 60 °C and reduced at 120 °C for 3 h in an H_2 flow (50 mL min^{-1}), which was denoted as Au/meso-Fe_2O_3.

3.2. Oxidation of Benzylic Alcohols

The oxidation of benzylic alcohol was conducted in a 50 mL 3-neck round-bottom flask, employing the substrate (1 mmol), iron-based catalyst (100 mg) and dodecane (1 mmol) in 10 mL of diphenyl ether under flowing air (30 mL·min^{-1}) at 120 °C and 500 rpm stirring. The aliquots were taken periodically and analyzed by gas chromatograph-flame ionization detection (GC-FID) (Shimadzu 2010 GC-FID, Kyoto, Japan, separation capillary column: Agilent HP-5, 0.320 mm inner diameter, 30 m long, 0.25 μm film thickness, Palo Alto, CA, USA) using dodecane as the internal standard (Supplementary Materials).

4. Conclusions

In summary, Au/meso-Fe_2O_3 with a highly ordered mesoporous structure was successfully synthesized by using KIT-6 as a template through the hard template strategy and was applied for the oxidation of benzylic alcohols using molecular oxygen as the oxidant. The characterization results show that Au/meso-Fe_2O_3 has a uniform pore structure, where the specific surface area and average pore diameter of the catalyst could reach 97 m^2·g^{-1} and 9.1 nm, respectively. The catalytic system not only presents a high 1-phenylethanol oxidation activity, but it also shows an excellent activity and selectivity for benzylic alcohol oxidation, which was evidenced by the model β–O–4 linkage dimer oxidation. The Au/meso-Fe_2O_3 catalyst has a unique mesoporous structure and high specific surface area, which facilitates the mass transport of the lignin model compounds and enhances the catalytic performance of the heterogeneous oxidation processes. In addition, the Au/meso-Fe_2O_3 shows a good catalytic reusability. The structural framework of the as-prepared catalyst was not changed during 3 cyclic runs and shows an excellent catalytic performance. These results indicated that the heterogeneous catalyst Au/meso-Fe_2O_3 could be used as a highly efficient catalytic system for the degradation of lignin, which shows a great significance for lignin valorization to value-added low molecular weight aromatics.

Supplementary Materials: The following are available online at http://www.mdpi.com/2073-4344/9/9/754/s1.

Author Contributions: Conceptualization and methodology, Y.J. and H.C.; Investigation and writing—original draft preparation, Y.J.; writing—review and editing, Y.J. and H.C.

Funding: This research was funded by the Key Research and Development Program of Tianjin, grant number 19YFSLQY00060.

Conflicts of Interest: The authors declare no conflict of interest.

References

1. Schutyser, W.; Renders, T.; Van den Bosch, S.; Koelewijn, S.F.; Beckham, G.T.; Sels, B.F. Chemicals from lignin: An interplay of lignocellulose fractionation, depolymerisation, and upgrading. *Chem. Soc. Rev.* **2018**, *47*, 852–908. [CrossRef]
2. Sheldon, R.A. Green and sustainable manufacture of chemicals from biomass: State of the art. *Green Chem.* **2014**, *16*, 950–963. [CrossRef]
3. Jiang, Z.; Zhao, P.; Hu, C. Controlling the cleavage of the inter- and intra-molecular linkages in lignocellulosic biomass for further biorefining: A review. *Bioresour. Technol.* **2018**, *256*, 466–477. [CrossRef] [PubMed]

4. Sun, Z.; Fridrich, B.; de Santi, A.; Elangovan, S.; Barta, K. Bright side of lignin depolymerization: Toward new platform chemicals. *Chem. Rev.* **2018**, *118*, 614–678. [CrossRef] [PubMed]
5. Teong, S.P.; Yi, G.; Zhang, Y. Hydroxymethylfurfural production from bioresources: Past, present and future. *Green Chem.* **2014**, *16*, 2015–2026. [CrossRef]
6. Zhang, X.; Wang, T.; Zhang, Q.; Xu, Y.; Long, J.; Chen, L.; Wang, C.; Ma, L. Production of alkanes from lignin-derived phenolic compounds over in situ formed Ni catalyst with solid acid. *Chem. Lett.* **2015**, *44*, 648–650. [CrossRef]
7. Behling, R.; Valange, S.; Chatel, G. Heterogeneous catalytic oxidation for lignin valorization into valuable chemicals: What results? What limitations? What trends? *Green Chem.* **2016**, *18*, 1839–1854. [CrossRef]
8. Huber, G.W.; Iborra, S.; Corma, A. Synthesis of transportation fuels from biomass: Chemistry, catalysts, and engineering. *Chem. Rev.* **2006**, *106*, 4044–4098. [CrossRef]
9. Upton, B.M.; Kasko, A.M. Strategies for the conversion of lignin to high-value polymeric materials: Review and perspective. *Chem. Rev.* **2016**, *116*, 2275–2306. [CrossRef]
10. Das, L.; Kolar, P.; Sharma-Shivappa, R. Heterogeneous catalytic oxidation of lignin into value-added chemicals. *Biofuels* **2012**, *3*, 155–166. [CrossRef]
11. Deng, W.P.; Zhang, H.X.; Wu, X.J.; Li, R.S.; Zhang, Q.H.; Wang, Y. Oxidative conversion of lignin and lignin model compounds catalyzed by CeO_2-supported Pd nanoparticles. *Green Chem.* **2015**, *17*, 5009–5018. [CrossRef]
12. Mottweiler, J.; Puche, M.; Raeuber, C.; Schmidt, T.; Concepcion, P.; Corma, A.; Bolm, C. Copper- and vanadium-catalyzed oxidative cleavage of lignin using dioxygen. *ChemSusChem* **2015**, *8*, 2106–2113. [CrossRef] [PubMed]
13. Sturgeon, M.R.; O'Brien, M.H.; Ciesielski, P.N.; Katahira, R.; Kruger, J.S.; Chmely, S.C.; Hamlin, J.; Lawrence, K.; Hunsinger, G.B.; Foust, T.D. Lignin depolymerisation by nickel supported layered-double hydroxide catalysts. *Green Chem.* **2014**, *16*, 824–835. [CrossRef]
14. Kruger, J.S.; Cleveland, N.S.; Zhang, S.; Katahira, R.; Black, B.A.; Chupka, G.M.; Lammens, T.; Hamilton, P.G.; Biddy, M.J.; Beckham, G.T. Lignin depolymerization with nitrate-intercalated hydrotalcite catalysts. *ACS Cata.* **2016**, *6*, 1316–1328. [CrossRef]
15. Wu, X.; Guo, S.; Zhang, J. Selective oxidation of veratryl alcohol with composites of Au nanoparticles and graphene quantum dots as catalysts. *Chem. Commun.* **2015**, *51*, 6318–6321. [CrossRef] [PubMed]
16. Luc, W.; Jiao, F. Synthesis of nanoporous metals, oxides, carbides, and sulfides: Beyond nanocasting. *Acc. Chem. Res.* **2016**, *49*, 1351–1358. [CrossRef] [PubMed]
17. Kleitz, F.; Choi, S.H.; Ryoo, R. Cubic Ia3d large mesoporous silica: Synthesis and replication to platinum nanowires, carbon nanorods and carbon nanotubes. *Chem. Commun.* **2003**, *17*, 2136–2137. [CrossRef] [PubMed]
18. Geng, L.; Zheng, B.; Wang, X.; Zhang, W.; Wu, S.; Jia, M.; Yan, W.; Liu, G. Fe_3O_4 nanoparticles anchored on carbon serve the dual role of catalyst and magnetically recoverable entity in the aerobic oxidation of alcohols. *ChemCatChem* **2016**, *8*, 805–811. [CrossRef]
19. Yang, X.; Huang, C.; Fu, Z.; Song, H.; Liao, S.; Su, Y.; Du, L.; Li, X. An effective pd-promoted gold catalyst supported on mesoporous silica particles for the oxidation of benzyl alcohol. *Appl. Catal. B Environ.* **2013**, *140*, 419–425. [CrossRef]
20. Bingwa, N.; Patala, R.; Noh, J.-H.; Ndolomingo, M.J.; Tetyana, S.; Bewana, S.; Meijboom, R. Synergistic effects of gold-palladium nanoalloys and reducible supports on the catalytic reduction of 4-nitrophenol. *Langmuir* **2017**, *33*, 7086–7095. [CrossRef]
21. Mobley, J.K.; Crocker, M. Catalytic oxidation of alcohols to carbonyl compounds over hydrotalcite and hydrotalcite-supported catalysts. *RSC Adv.* **2015**, *5*, 65780–65797. [CrossRef]
22. Martinez-Gonzalez, S.; Gomez-Aviles, A.; Martynyuk, O.; Pestryakov, A.; Bogdanchikova, N.; Cortes Corberan, V. Selective oxidation of 1-octanol over gold supported on mesoporous metal-modified hms: The effect of the support. *Catal. Today* **2014**, *227*, 65–70. [CrossRef]
23. Song, Y.; Mobley, J.K.; Motagamwala, A.H.; Isaacs, M.; Dumesic, J.A.; Ralph, J.; Lee, A.F.; Wilson, K.; Crocker, M. Gold-catalyzed conversion of lignin to low molecular weight aromatics. *Chem. Sci.* **2018**, *9*, 8127–8133. [CrossRef] [PubMed]

24. Yin, S.; Li, J.; Zhang, H. Hierarchical hollow nanostructured core@shell recyclable catalysts gamma-Fe_2O_3@LDH@Au_{25-x} for highly efficient alcohol oxidation. *Green Chem.* **2016**, *18*, 5900–5914. [CrossRef]
25. Rakap, M.; Ozkar, S. Hydroxyapatite-supported palladium(0) nanoclusters as effective and reusable catalyst for hydrogen generation from the hydrolysis of ammonia-borane. *Int. J. Hydrog. Energ.* **2011**, *36*, 7019–7027. [CrossRef]
26. Liu, Y.; Tsunoyama, H.; Akita, T.; Xie, S.; Tsukuda, T. Aerobic oxidation of cyclohexane catalyzed by size-controlled au clusters on hydroxyapatite: Size effect in the sub-2 nm regime. *ACS Cata.* **2011**, *1*, 2–6. [CrossRef]
27. Baker, T.A.; Liu, X.; Friend, C.M. The mystery of gold's chemical activity: Local bonding, morphology and reactivity of atomic oxygen. *Phy. Chem. Chem. Phy.* **2011**, *13*, 34–46. [CrossRef] [PubMed]
28. Ge, J.; Hu, Y.; Biasini, M.; Beyermann, W.P.; Yin, Y. Superparamagnetic magnetite colloidal nanocrystal clusters. *Angew. Chem. Int. Edit.* **2007**, *46*, 4342–4345. [CrossRef]
29. Megias-Sayago, C.; Chakarova, K.; Penkova, A.; Lolli, A.; Ivanova, S.; Albonetti, S.; Cavani, F.; Antonio Odriozola, J. Understanding the role of the acid sites in 5-hydroxymethylfurfural oxidation to 2,5-furandicarboxylic acid reaction over gold catalysts: Surface investigation on $Ce_xZr_{1-x}O_2$ compounds. *ACS Cata.* **2018**, *8*, 11154–11164. [CrossRef]
30. Ma, R.; Xu, Y.; Zhang, X. Catalytic oxidation of biorefinery lignin to value-added chemicals to support sustainable biofuel production. *ChemSusChem* **2015**, *8*, 24–51. [CrossRef]
31. Wang, S.; Yin, S.; Chen, G.; Li, L.; Zhang, H. Nearly atomic precise gold nanoclusters on nickel-based layered double hydroxides for extraordinarily efficient aerobic oxidation of alcohols. *Catal. Sci. Technol.* **2016**, *6*, 4090–4104. [CrossRef]
32. Masunga, N.; Tito, G.S.; Meijboom, R. Catalytic evaluation of mesoporous metal oxides for liquid phase oxidation of styrene. *Appl. Catal. A Gen.* **2018**, *552*, 154–167. [CrossRef]
33. Nishimura, S.; Yakita, Y.; Katayama, M.; Higashimine, K.; Ebitani, K. The role of negatively charged au states in aerobic oxidation of alcohols over hydrotalcite supported aupd nanoclusters. *Catal. Sci. Technol.* **2013**, *3*, 351–359. [CrossRef]
34. Xu, J.; Liu, Y.; Wu, H.; Li, X.; He, M.; Wu, P. Ets-10 supported Au nanoparticles for solvent-free oxidation of 1-phenylethanol with oxygen. *Catal. Lett.* **2011**, *141*, 860–865. [CrossRef]
35. Haider, P.; Grunwaldt, J.-D.; Baiker, A. Gold supported on mg, al and cu containing mixed oxides: Relation between surface properties and behavior in catalytic aerobic oxidation of 1-phenylethanol. *Catal. Today* **2009**, *141*, 349–354. [CrossRef]
36. Wang, L.; Meng, X.; Xiao, F. Au nanoparticles supported on a layered double hydroxide with excellent catalytic properties for the aerobic oxidation of alcohols. *Chin. J. Catal.* **2010**, *31*, 943–947. [CrossRef]
37. Li, L.; Dou, L.; Zhang, H. Layered double hydroxide supported gold nanoclusters by glutathione-capped Au nanoclusters precursor method for highly efficient aerobic oxidation of alcohols. *Nanoscale* **2014**, *6*, 3753–3763. [CrossRef]
38. Ballarin, B.; Barreca, D.; Boanini, E.; Cassani, M.C.; Dambruoso, P.; Massi, A.; Mignani, A.; Nanni, D.; Parise, C.; Zaghi, A. Supported gold nanoparticles for alcohols oxidation in continuous flow heterogeneous systems. *ACS Sustain. Chem. Eng.* **2017**, *5*, 4746–4756. [CrossRef]
39. Buonerba, A.; Cuomo, C.; Sanchez, S.O.; Canton, P.; Grassi, A. Gold nanoparticles incarcerated in nanoporous syndiotactic polystyrene matrices as new and efficient catalysts for alcohol oxidations. *Chem. Eur. J.* **2012**, *18*, 709–715.
40. Asao, N.; Hatakeyama, N.; Menggenbateer; Minato, T.; Ito, E.; Hara, M.; Kim, Y.; Yamamoto, Y.; Chen, M.; Zhang, W.; et al. Aerobic oxidation of alcohols in the liquid phase with nanoporous gold catalysts. *Chem. Commun.* **2012**, *48*, 4540–4542. [CrossRef]
41. Rinesch, T.; Mottweiler, J.; Puche, M.; Concepcion, P.; Corma, A.; Bolm, C. Mechanistic investigation of the catalyzed cleavage for the lignin β-O-4 linkage: Implications for vanillin and vanillic acid formation. *ACS Sustain. Chem. Eng.* **2017**, *5*, 9818–9825. [CrossRef]
42. Tsang, A.S.K.; Kapat, A.; Schoenebeck, F. Factors that control c-c cleavage versus c-h bond hydroxylation in copper-catalyzed oxidations of ketones with O_2. *J. Am. Chem. Soc.* **2016**, *138*, 518–526. [CrossRef] [PubMed]

43. Song, Q.; Cai, J.; Zhang, J.; Yu, W.; Wang, F.; Xu, J. Hydrogenation and cleavage of the C-O bonds in the lignin model compound phenethyl phenyl ether over a nickel-based catalyst. *Chin. J. Catal.* **2013**, *34*, 651–658. [CrossRef]
44. Sun, X.; Shi, Y.; Zhang, P.; Zheng, C.; Zheng, X.; Zhang, F.; Zhang, Y.; Guan, N.; Zhao, D.; Stucky, G.D. Container effect in nanocasting synthesis of mesoporous metal oxides. *J. Am. Chem. Soc.* **2011**, *133*, 14542–14545. [CrossRef] [PubMed]